Comparison of ANN and DoE for the prediction of laser machined micro-channel dimensions

S.M. Karazi [1,*], A. Issa [2] and D. Brabazon [3]

[1] shadi.karazi@dcu.ie, [2]ahmed.issa2@mail.dcu.ie, [3]dermot.brabazon@dcu.ie

School of Mechanical and Manufacturing Engineering, Dublin City University, Dublin, Ireland

Abstract

This paper presents four models developed for the prediction of the width and depth dimensions of CO_2 laser formed micro-channels in glass. A 3^3 statistical design of experiments (DoE) model was built and conducted with the power (P), pulse repetition frequency (PRF), and traverse speed (U) of the laser machine as the selected parameters for investigation. Three feed-forward, back-propagation Artificial Neural Networks (ANNs) models were also generated. These ANN models were varied to investigate the influence of variations in the number and the selection of training data. Model A was constructed with 24 data randomly selected from the experimental results, leaving three data points for model testing; Model B was constructed with the eight corner points of the experimental data space, and seven other randomly selected data, leaving 12 data points for testing; and Model C was constructed with 15 randomly selected data leaving 12 data points for testing. These models were developed separately for both micro-channel width and depth prediction. These ANN models were constructed in LabVIEW coding. The performance of these ANN models and the DoE model were compared. When compared with the actual results two of the ANN models showed greater average percentage error than the DoE model. The other ANN model showed an improved predictive capability that was approximately twice as good as that provided from the DoE model.

* Corresponding author. Tel.: +353 1 700 7674; fax: +353 1 700 5345.

E-mail address: shadi.karazi@dcu.ie (S. M. Karazi).

Keywords: ANN; DoE; laser micro-machining; prediction modelling; parameter selection; channel dimensions

1. Introduction

Laser micro-machining processes include the drilling, cutting, milling and engraving of materials with micro-dimensional tolerances. In spite of the fact that laser micro-machining is a technically complex manufacturing process, research work has enabled the fabrication of increasingly precise, smooth, and clean components at high speed [1-3]. Laser micro-machining is used for micro-channel and micro-electromechanical system production within many applications. These include telecommunications, glass cutting, micro-sensors [4-6]; micro-via, ink jet printer nozzles, biomedical catheter drilling, thin-film scribing [7]; micro-fluidic channels for blood/protein analysis [8]; optical vibration sensors [9]; three-dimensional binary data storage [10-12]; and novelty fabrications [13].

In order to find a set of laser processing parameters that provides the required micro-channel dimensions for a specific application under particular processing constraints, predictive models can be used. Several statistical and numerical approaches have been utilised to predict and optimise various laser manufacturing processes including Artificial Neural Networks (ANN) [14]; genetic algorithms [15], design of experiments [3], finite elements analysis [16], ant colony optimisation [17], and fuzzy logic [18]. Due to their non-linear, adaptive and learning ability using collected data, ANN models have been successfully applied to a large number of problems in several domain applications. Many researchers have for example applied DoE, evolutional algorithms and ANN techniques in the area of laser welding [19-21]. ANN mathematical models are a type of Artificial Intelligence (AI) originally designed to mimic the massively parallel operations of the human brain and aspects of how we believe the brain works. Neural network nodal functions can be evaluated simultaneously, thereby gaining enormous increases in processing speed [22]. A neural network can be considered as a black box that is able to

predict an output pattern when it recognizes a given input pattern. Once trained, the neural network is able to recognize similarities when presented with a new input pattern, resulting in a predicted output pattern [23]. Back-propagation neural network algorithms have been successfully applied by Drugos et al. to predict and improve the selection of the number of laser passes required for an automated laser sheet metal bending of aluminium and steel [24]. Lee et al. used ANN modelling to predict the process outputs from the stereolithography rapid prototyping process [14].

In recent work by Dhupal et al., these workers incorporated experimental observations of an Nd:YAG laser machining system into an ANN model for predicting parameter settings to achieve precise micro-grooving operations on Al_2TiO_5. In this model, a multilayered feed forward neural network was combined with DoE optimisation to enable prediction of the desired outputs of laser micro-grooves. Neurons in the input layer corresponded to air pressure, lamp current, pulse frequency, pulse width and cutting speed. The output layer corresponded to the responses such as the width at the bottom and top sections, and depth of the micro-groove. A maximum of 5% prediction error was observed between the results based on the ANN predictive model and the actual experimental observations [25].

Yousef et al. used artificial neural networks ANNs to model and analyse the material removal process. In their work these authors wanted to develop a model which they could use to select the laser processing parameters which would result in the required ablation depth and width of a conical shaped crater. The test results showed that the ANN modelled level of pulse energy corresponding to specific depth and diameter was consistent with the actual level of pulse energy to a high degree of accuracy due to the adaptive properties of ANN [26].

Setia et al. used back-propagation ANNs to model micro-fluidic via formation using laser ablation. Genetic algorithms were utilized in conjunction with the ANN models to determine the input parameters for a specific channel dimensional requirement. Experimental verification demonstrated that the models produced allow for input parameter selection such that targeted dimensional accuracy of the ablation was improved by as much

as 40% for the ablated film thickness, 30% for via diameter, 9%for via wall angle, and more than 100% for via resistance [27].

Zurek et al. wrote a detailed ANN code in LabVIEW, called ANETka, and used it to investigate the magnetic properties of magnetic cores. This code allows the generation of ANN models that are fully interconnected and of feed-forward structure with error back-propagation algorithm. This program allows a maximum of eight layers and 100 neurons per layer. Three activation functions (linear, sigmoid and tangent hyperbolic) are selectable with automatic data linear normalising between 0.05 and 0.95. This code effectively controls the training phase of the ANN in order to reach a selected Root Mean Square (RMS) error. This allows ANN models with very high degree of accuracy to be reached [28, 29]. ANETka is working according to error back-propagation learning. That consists of two passes through the different layers of the network: a forward pass and a backward pass. In the forward pass, an input vector is applied to the input layer of the network, and its effect propagates through the network layer by layer. Finally, a set of outputs is produced as the actual response of the network. During the forward pass the synaptic weights of the networks are all fixed. During the backward pass, on the other hand, the synaptic weights are all adjusted in accordance with an error-correction rule. Specifically, the actual response of the network is subtracted from a desired (target) response to produce an error signal. This error signal is then propagated backward through the network against the direction of synaptic connections-hence the name "error back-propagation." The synaptic weights are adjusted to make the actual response of the network move closer to the desired response in a statistical sense [30].

The prediction of the dimensions of the laser micro-machining channels is an important requirement for optimisation of the laser control parameters. A CO_2 laser micro-machining system was used by the current authors for the production of micro-channels [3]. Based on the intensity range used in the experimental work presented in this paper, the induced laser absorption is of the laser supported combustion type. Energy is deposited into the material by the laser pulse and is transported out of the irradiated region by thermal diffusion. In this case, the relative rate of energy deposition and thermal diffusion determines the damage

threshold. Dependence of the breakdown threshold on the presence of impurity electrons in the conduction band also makes the threshold for optical breakdown and damage somewhat probabilistic or non-deterministic [31]. Plasma is initiated at the target's surface, whose temperature can exceed 10^4 K, during the ablative interaction [32]. All of these factors combined make it difficult to produce models which accurately predict the geometry of channels produced during the laser micro-machining process. DoE and ANN models that were developed and implemented are presented below. These relate the input laser processing parameters (power, traverse speed and pulse repetition frequency) to the output responses (machined channel width and depth). The DoE and ANN models may be used to select the input parameters for required output dimensions or to predict the dimensions of the channels based on set inputs. Direct comparisons between the predictive accuracies of the ANN and DoE models are drawn.

2. Experiments

2.1 Laser micro-machining and DoE model setup

A series of experiments were performed to determine the relationship between the main laser emission parameters of a CO_2 laser and the dimensions of corresponding produced micro-channels. After initial screening experiments, a factorial design of experiments was conducted to analyse the outcomes of these laser processing parameters on the resulting micro-channels' dimensions. Three process parameters analysed in this work were the laser power, pulse repetition frequency and translation speed of the glass sample. Each of these were analysed at three levels in the form of a 3^3 factorial design of experiments. The low, middle and high levels chosen for power, pulse repetition frequency and traverse speed are shown in Table 1. The low level is represented by -1, the middle by 0 and the high level by 1. A slightly off centre value of 228 Hz was chosen for the pulse repetition frequency. This is coded as -0.433 for the design of experiments which represents the degree of shift from the central position for this parameter. This shift from the central position was due to hardware capabilities of the laser machine. There are 27 possible combinations of the three

process parameters at the three levels. Table 2 shows a list of these 27 combinations of the laser control parameters that were used in the conducted experiments. The width and depth of every channel were measured. Each of these experiments was performed three times to get an average value of these surface topography characteristics and an indication of the degree of repeatability.

Table 1: Control parameters levels and their corresponding DoE coding

	Actual			**Coded**		
	Low	**Mid**	**High**	**Low**	**Mid**	**High**
P (W)	18	24	30	-1	0	1
PRF (Hz)	160	228	400	-1	-0.433	1
U (mm/min)	100	300	500	-1	0	1

Table 2: List of laser control parameter of the experiments performed. Experiment number 14 represents the experimental conditions repeated five times for repeatability analysis

#	**P**	**PRF**	**U**	**#**	**P**	**PRF**	**U**	**#**	**P**	**PRF**	**U**
1	18	160	100	**10**	24	160	100	**19**	30	160	100
2	18	160	300	**11**	24	160	300	**20**	30	160	300
3	18	160	500	**12**	24	160	500	**21**	30	160	500
4	18	228	100	**13**	24	228	100	**22**	30	228	100
5	18	228	300	**14**	24	228	300	**23**	30	228	300
6	18	228	500	**15**	24	228	500	**24**	30	228	500
7	18	400	100	**16**	24	400	100	**25**	30	400	100
8	18	400	300	**17**	24	400	300	**26**	30	400	300
9	18	400	500	**18**	24	400	500	**27**	30	400	500

For variability analysis, five additional experiments were repeated at the middle point of the investigated ranges, such that the total number of experiments conducted was 32 ($=3^3+5$). Fig. 1 shows the distribution of process control parameter data in 3D data space.

The width and depth dimensions of the micro-channels for each experiment were measured at three different locations along the produced channel. The measurement system used was an in-house built laser profilometer that had a 1.95 μm resolution in the x and y direction and a 0.5 μm resolution in the z-direction [3]. Average values and 95% confidence intervals for these were determined. Fig. 2 shows a schematic of a micro-channel depicting the studied outcomes.

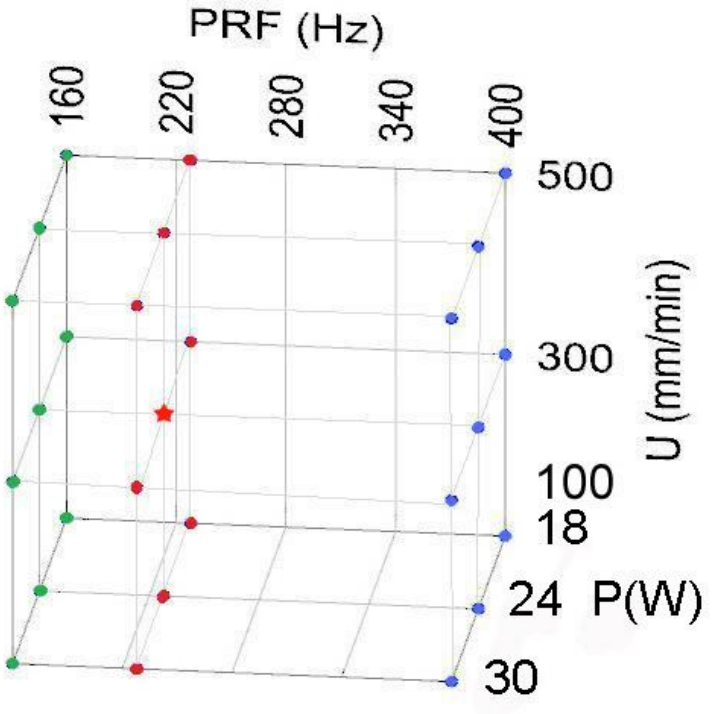

Fig. 1: 3D representation of the process control parameters' points investigated.
★ indicates where five additional experiments were repeated.

The point pair, between which the width was measured, was picked using the cursors and by looking at all views of the channel. In some channel scans, the build up zone was higher than the unprocessed glass surface. Generally, the unprocessed glass surface was first found by moving the cursors in the z-direction when viewing the scanned surface edge in the direction of the x-axis. Then the channel's isometric view was examined and the cursors

moved again in the x and y-direction until the locations defining the highest points on opposite edges of the channel were found. This pair of points was recorded and the displacement between them was recorded as the channel width. This procedure was repeated for three different locations along the channel axis and the average was calculated. A similar procedure was followed to record the channel depth.

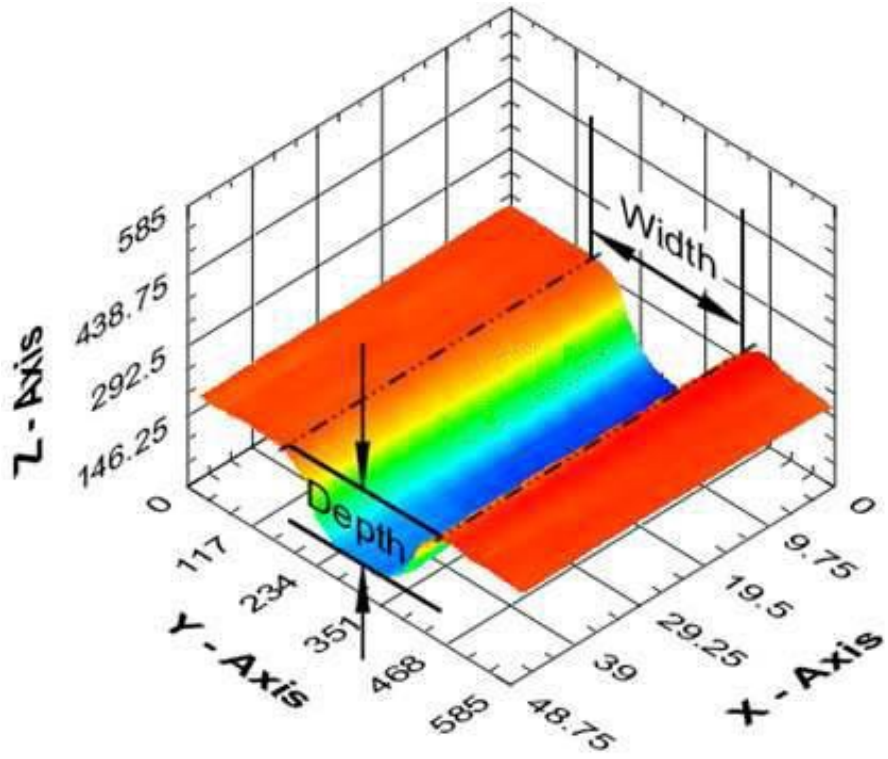

Fig. 2: Micro-channel schematic indicating the measured micro channel's width and depth.

2.2 Setup of ANN models

The average dimensional measurement results (27 for width and 27 for depth) provided the data from which training sets were chosen. Three ANN models (A, B and C) were developed for the width and the depth. All ANN models had the three inputs P, U and PRF. In order to determine the effect of training data on model predictive capability, each of these three models was based on different sets of training and testing data as follows.

- Model A: 24 randomly selected experiments (from the total of 27) were used as a data set to train the network and the other three experiments were used as test data;
- Model B: the experiments from the eight corner points from the experimental data space and seven randomly selected experiments (15 in total) were used to train the network and the other 12 experiments were used as test data;
- Model C: 15 randomly selected experiments were used as the data set to train the network and the other 12 experiments were used as test data.

Test data were used for verification purposes in order to evaluate the predictive capabilities of the ANN models. Fig. 3 shows a representation of the training data distribution in 3D space, for (a) model A, (b) model B and (c) model C. The number of data available for training and testing was limited in this work to the 27 data points which were available. The selection of the production parameters, fabrication of the channels and the measurement of the channels dimensions took approximately three months [3, 33]. The percentage of test data to overall data was set to a low level for model A compared to model B and C. This number of test data is much less than would normally be used for generating ANN models. This data was however chosen from the limited data available in order to compare the predication capability of the Design of Experiments model to various possible settings in the ANN models.

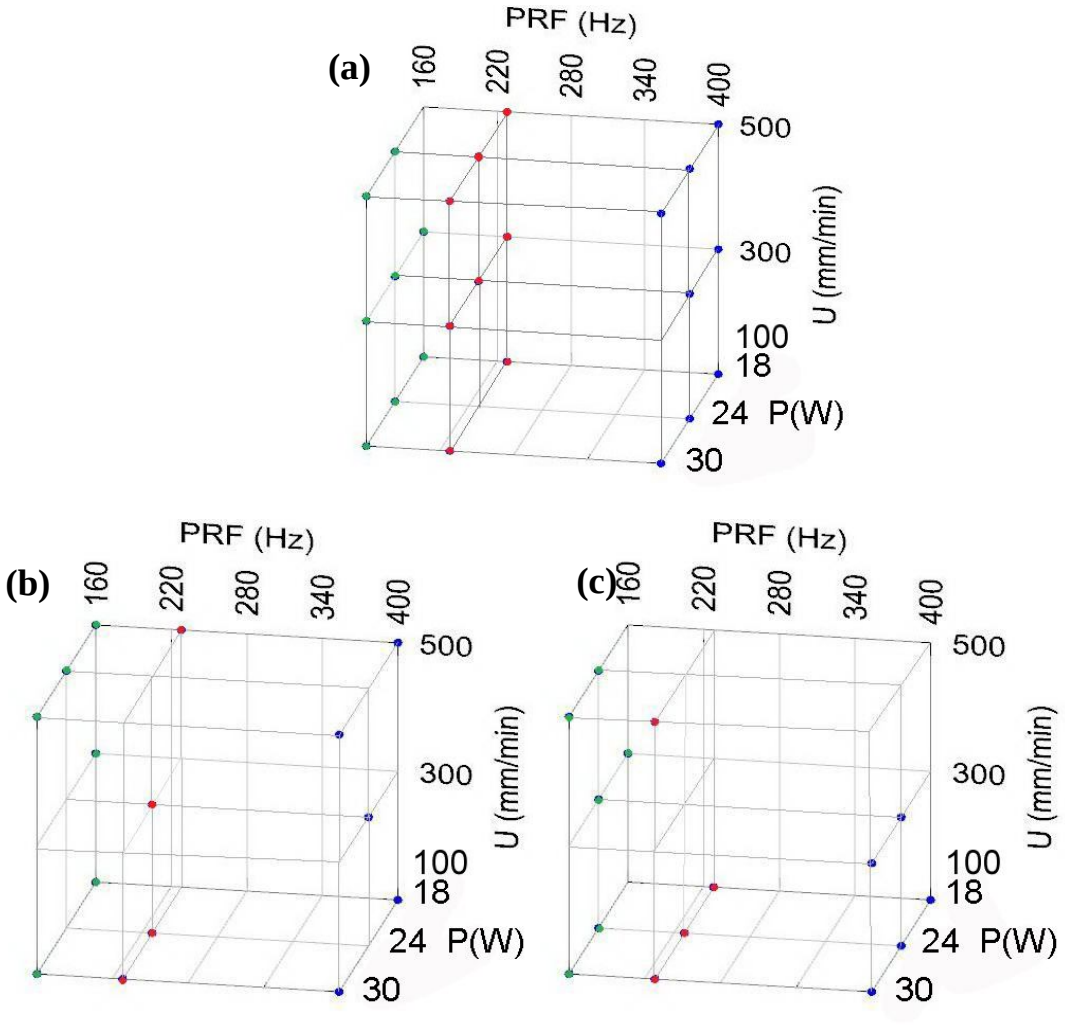

Fig. 3: Representation of the training data for (a) model A, (b) model B and (c) model C.

2.3 Configuration of ANN

The models examined in this work were designed and run with the ANETka software in feed-forward back-propagation ANN mode. Due to the absence of a quantifiable method for a priori evaluation of the best network architecture, intensive trial and error examination was carried out in order to optimise the configuration of the ANN. Two ASCII text spreadsheet input files were used for each model. The first one contained the training data inputs and corresponding outputs for the training stage. The second one contained the test data inputs and their outputs for the verification stage. As indicated in last paragraph of the introduction, laser micro-machining process is a very complicated process for which to

produce an accurate predictive model. Therefore the number of hidden layers were varied between one and three in order to investigate the number of layers required to model the process. The number of nodes (neurons) in each of hidden layers was varied between four to 80 neurons. A schematic description of these investigation schema layers are shown in Fig. 4.

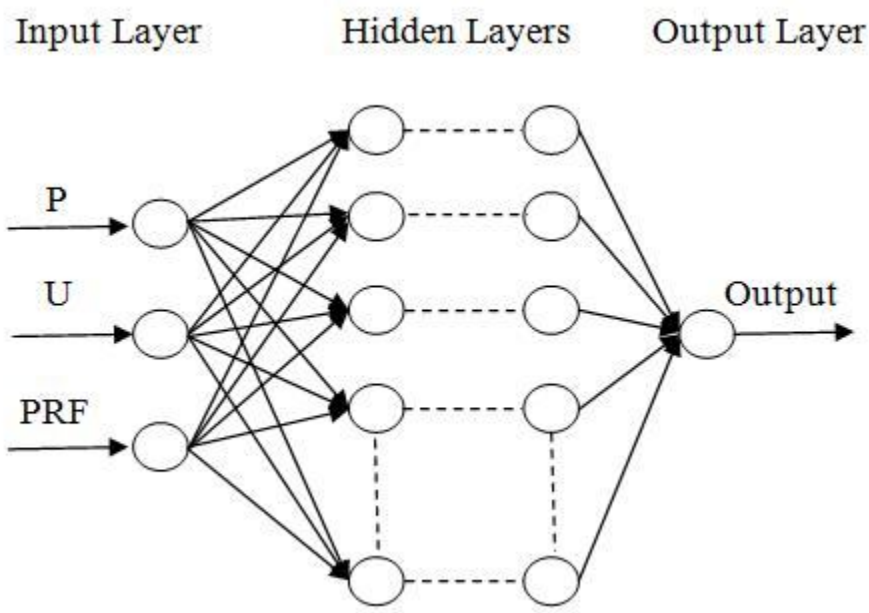

Fig. 4: Architecture of feed-forward ANN schema developed with three inputs and one output.

Inputs and outputs were normalized in the range of 0.05–0.95. A transfer sigmoid function was used in all layers except the input layer as this nonlinear function has good generalisation capability. The learning rate parameter was set during simulation to control the magnitude of weight and bias updates. The selection of this value significantly affected the training time of the ANN. The programme iteratively presented the training data one by one to the ANN, and the weights automatically corrected after each case. Another parameter, the momentum value was used to decrease the likeliness of the simulation becoming stuck in local optima. Experimentally the learning rate was manually set at a value between 0.0001 and 6.0000 depending on the simulation during training process and the momentum was fixed at a medium value of 0.8 for all ANN models. In an effort to

minimise the training error and avoid over training, the training process was supervised during the ANN model formulation. During this training process, the ANETka software was used to provide a graphical record of the past and current RMS error value. This was continuously monitored so that good prediction capability of the models could be achieved. Models for which the RMS error increased during training were discarded. The process of model generation was then re-initialised to produce the final ANN model. Only models with RMS error below 0.001% were accepted. The number of iterations was kept as low as possible during formulation of the ANN model.

3. Results

3.1. Micrographs of produced channels

Micrographs highlighting the width of the produced micro-channels are shown in Fig. 5. Fig. 5 a, b and c show channels produced at 18 W, 24 W and 30 W respectively. The corresponding and increasing channel widths were respectively 222, 267 and 310 mm. The PRF and U were fixed at 228 Hz and 500 mm/min for production of these channels. Increasing power results in an increase of pulse energy and fluence which lead to an increased channel width and depth.

Fig. 5 d, e and f show channels produced at 160, 228 and 400 Hz respectively. The corresponding and decreasing channel widths were 314, 267 and 187 mm. The P and U were fixed at 24 W and 500 mm/min for production of these channels. Pulse energy is calculated as the average power divided by the pulse repetition frequency, PRF. This inverse relationship shows that higher PRF produced lower pulse energy and fluence which in turn resulted in decreased channel width and depth.

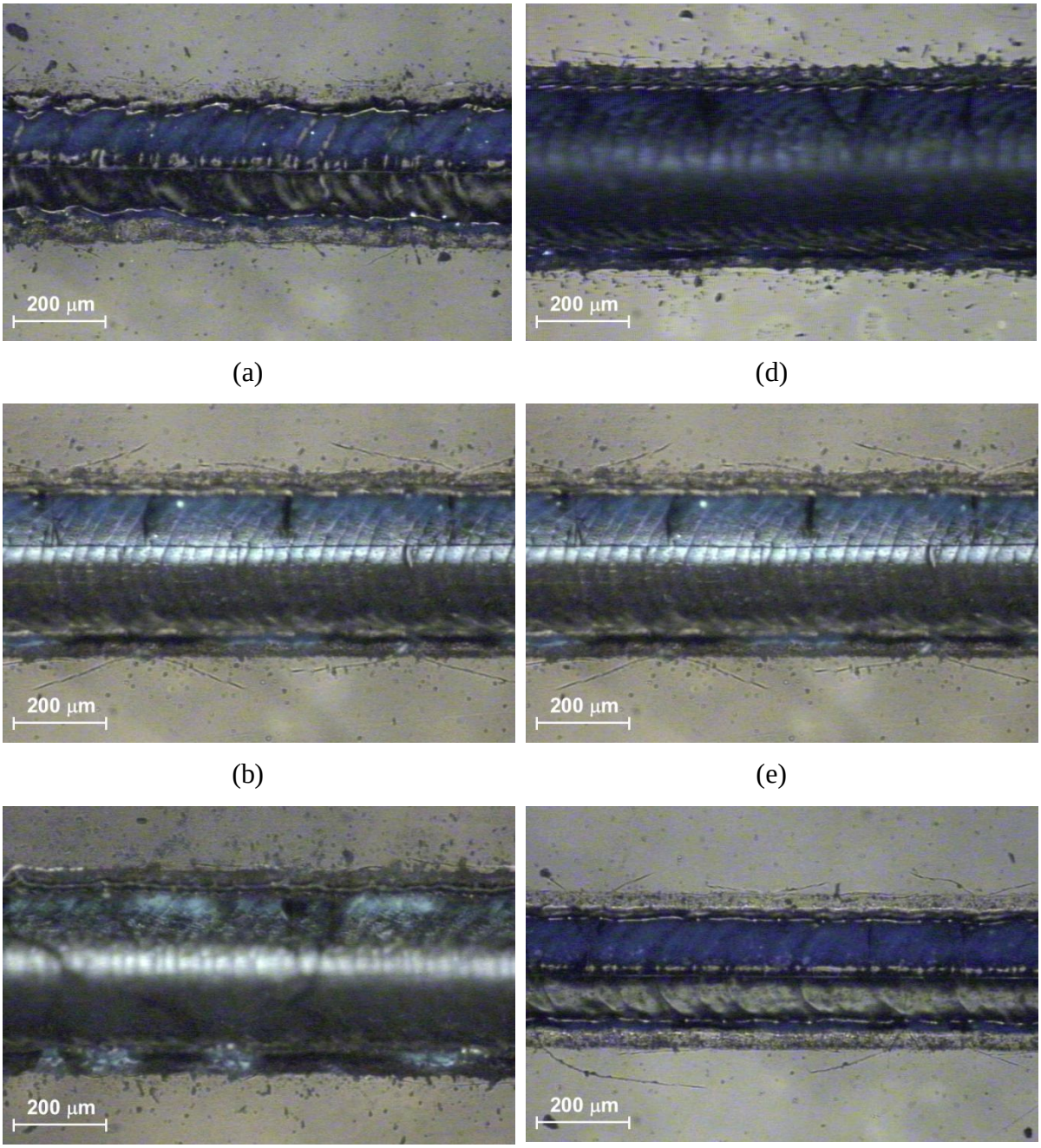

Fig. 5: Micrographs of top down view showing width of micro-channels produced with increasing power (a) channel number 6 at 18 W, (b) channel number 15 at 24W, (c) channel number 24 at 30 W, and increasing PRF (d) channel number 12 at 160 Hz, (e) channel number 15 at 228 Hz, and (f) channel number 18 at 400 Hz.

3.2. ANN vs DoE for predicting width and depth dimensions

After testing a large variety of hidden layer variations it was found that the most accurate ANN model schemas in this work were achieved with one hidden layer. This may be expected as multiple hidden layers are used for models of a deeply complex nature where response surfaces are of a higher order non-linear response [30]. Table 3 shows the number of nodes in the hidden layer that achieved the most accurate predictions of width and depth for models A, B and C.

Table 3: Number of nodes in the hidden layer for width and depth models in A, B, and C models

Model	**A**	**B**	**C**
Width	6	20	80
Depth	6	10	4

The actual and predicted values of width and depth are shown in Table 4. The bold numbers indicate accurately predicted values. In the penultimate row of Table 4, average percentage errors are shown. The percentage error (e_i) was calculated according to the formula:

$$e_i = 100 * \frac{(\text{predicted value} - \text{actual value})}{\text{actual value}} \%.$$

The last row in Table 4 shows the absolute maximum percentage error, E_∞, which indicates the worst prediction error for each model. In this case, E_∞ is very beneficial as the largest deviation allowable in laser micro-machining applications is often limited to a maximum allowable amount of error.

$$E_\infty = \max_{i=1}^{n} |e_i|$$

It can be seen from the last two rows in Table 4 that model B produced the lowest average percentage error and model A produced the smallest absolute maximum percentage error. In Table 4, the ability of the models to predict the training data as well as the test data is shown. The ability of the models to predict the test data indicates the generalisation of the

models as these test data were not used in the formation of these models. The generalisation of model B can be seen to be better than model A or model C in that it has predicted more accurately the actual channels' widths and depths. This can be seen by comparing the individual predictions and more clearly by comparing the overall percentage errors in the penultimate last row of this Table.

Table 4: Actual vs. predicted from width and depth models in A, B, C, and DoE models

#	Width					Depth				
	Actual	A	B	C	DoE	Actual	A	B	C	DoE
1	315	**315.00**	**315.00**	309.03	314.57	213	**213.00**	**213.00**	199.59	210.95
2	308	**308.00**	**308.00**	**308.00**	308.28	135	**135.00**	**135.00**	**135.00**	132.09
3	302	294.79	**302.00**	297.82	**302.00**	74	71.34	**74.00**	73.18	72.71
4	248	**248.00**	242.47	**248.00**	249.76	120	**120.00**	118.38	**120.00**	123.51
5	231	**231.00**	240.04	251.14	234.28	45	**45.00**	54.47	68.71	61.34
6	222	**222.00**	**222.00**	248.21	218.80	21	**21.00**	**21.00**	34.00	18.66
7	163	**163.00**	**163.00**	**163.00**	158.84	26	**26.00**	**26.00**	**26.00**	23.70
8	118	**118.00**	116.21	162.96	120.10	13	**13.00**	9.65	12.48	3.75
9	81	**81.00**	**81.00**	162.82	81.36	3	**3.00**	**3.00**	8.69	3.29
10	320	**320.00**	335.67	**320.00**	318.63	279	**279.00**	306.44	**279.00**	283.97
11	324	**324.00**	322.53	**324.00**	319.52	202	**202.00**	205.53	**202.00**	201.34
12	314	**314.00**	**314.00**	**314.00**	320.42	130	**130.00**	**130.00**	**130.00**	138.20
13	271	267.03	**271.00**	**271.00**	269.97	225	193.45	**225.00**	**225.00**	217.13
14	266	**266.00**	**266.00**	282.60	266.19	146	**146.00**	**146.00**	154.87	141.94
15	267	**267.00**	259.42	279.63	262.41	89	**89.00**	73.06	92.92	86.22
16	213	**213.00**	234.58	**213.00**	219.91	120	**120.00**	116.96	**120.00**	123.41
17	209	**209.00**	**209.00**	**209.00**	204.30	48	**48.00**	**48.00**	**48.00**	67.01
18	187	**187.00**	147.10	205.00	188.69	30	**30.00**	18.60	23.16	30.10
19	365	**365.00**	**365.00**	**365.00**	364.45	379	**379.00**	**379.00**	**379.00**	378.48
20	351	**351.00**	354.90	357.23	353.19	296	**296.00**	315.22	314.42	292.09
21	345	**345.00**	**345.00**	**345.00**	341.94	227	**227.00**	**227.00**	**227.00**	225.17
22	332	**332.00**	**332.00**	**332.00**	331.96	320	**320.00**	**320.00**	**320.00**	332.24
23	316	**316.00**	322.97	326.87	320.54	248	**248.00**	258.44	236.90	244.01
24	310	**310.00**	316.14	**310.00**	309.12	166	**166.00**	191.61	**166.00**	175.27
25	327	**327.00**	**327.00**	**327.00**	322.76	256	**256.00**	**256.00**	**256.00**	244.61
26	308	309.18	321.37	**308.00**	310.93	142	129.77	176.97	**142.00**	151.75
27	300	**300.00**	**300.00**	288.98	299.11	88	**88.00**	**88.00**	79.45	78.38
Average e_i		-0.13%	0.01%	6.61%	0.02%	-	-0.97%	-0.08%	10.09%	-0.33%
E_∞		2.4%	21.3%	101%	3.3%	-	14.0%	38.0%	189.6%	71.1%

3.3 Predicting the effect of control parameters on the outputs using ANN

In order to predict the interactive effect of the laser control parameters on the dimensions of the micro-channels, the list of laser control parameters' levels shown in Table 5 was used. Using all possible combinations of these data ($2197 = 13^3$) as input data to model B, the dimensions for the width and depth of the micro-channels were predicted. As an example of the output from the ANN model, Fig. 6 and Fig. 7 show the relation PRF and P, U and P, and PRF and U for the mid levels of the other parameters which were U=300 mm/min, PRF=280 Hz, and P=24W respectively. The results of this prediction demonstrate graphically the effect of changing two selected parameters on the dimensions of the micro-channels, while the third parameter was held constant at its average value. These figures offer a visual aid to select parameters or parameter ranges for a required output or output range. These graphs show simultaneously the combined effect of two parameters on the resulting dimension when the third parameter is held constant. Fig. 6 (a), for example, shows the effect of PRF and P on channel width. From this figure it can be seen that these two parameters interact with each other. The level of PRF selected for example, has an different effective output channel width response profile which is dependent on the input power setting. It can also be seen that as PRF decreases and P increases the resulting channel width increases. On the other hand, from Fig. 6 (b) it can be seen that there is no appreciable interaction between the traverse speed and the input power. This is due to the negligible effect of the speed in this case on the width of the channel.

Table 5: Laser control parameters' levels used to predict the interactive effect of the laser control parameters on the dimensions of the laser machined micro-channel

#	**1**	**2**	**3**	**4**	**5**	**6**	**7**	**8**	**9**	**10**	**11**	**12**	**13**
P (W)	18	19	20	21	22	23	24	25	26	27	28	29	30
PRF (Hz)	160	180	200	220	240	260	280	300	320	340	360	380	400
U (mm/min)	100	133	167	200	233	267	300	333	367	400	433	467	500

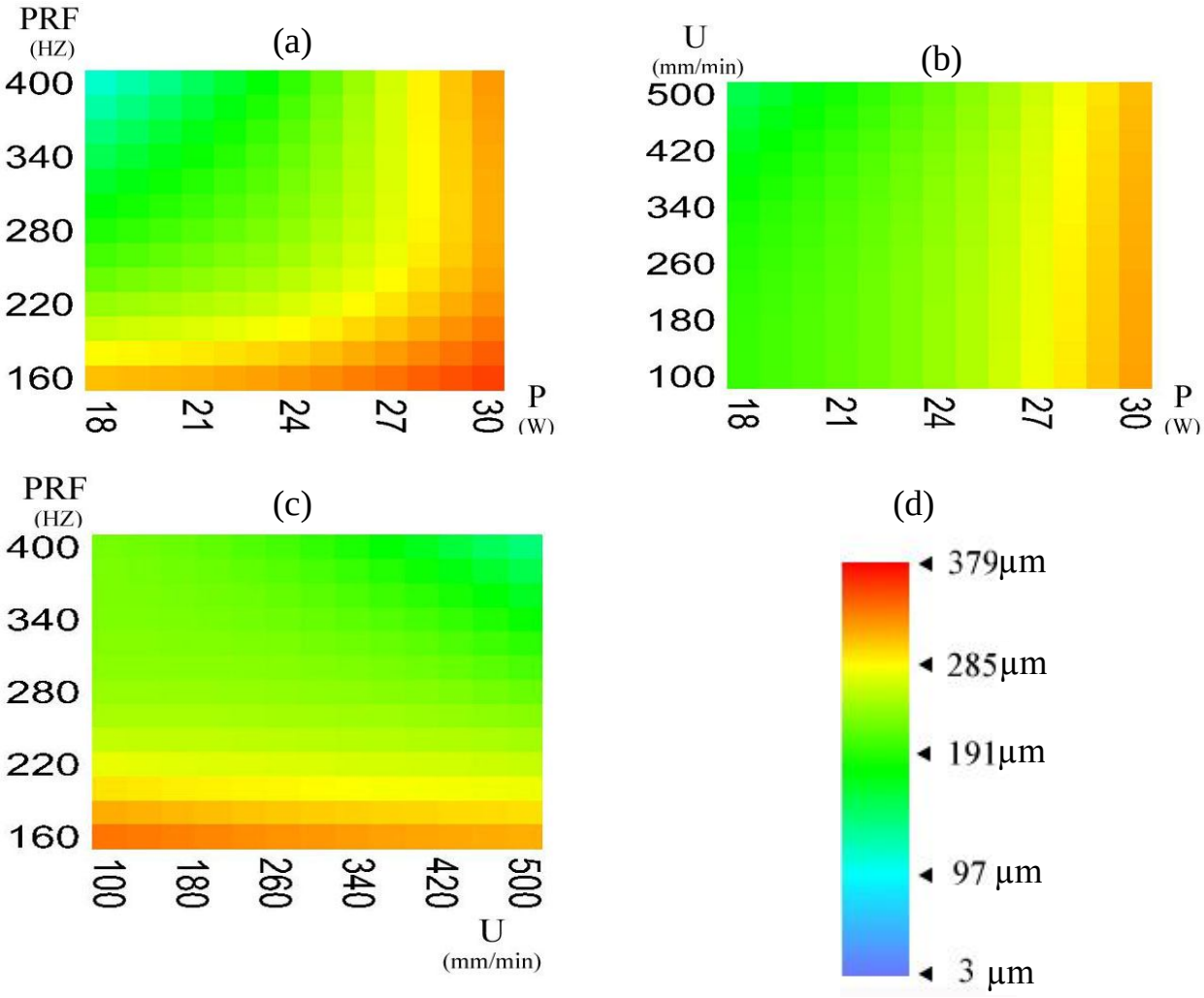

Fig. 6: Showing interactive effect on width level for (a) PRF and P with U=300 mm/min; (b) U and P with PRF=280 Hz; (c) PRF and U with P=24W; and (d) scale bar for dimensions.

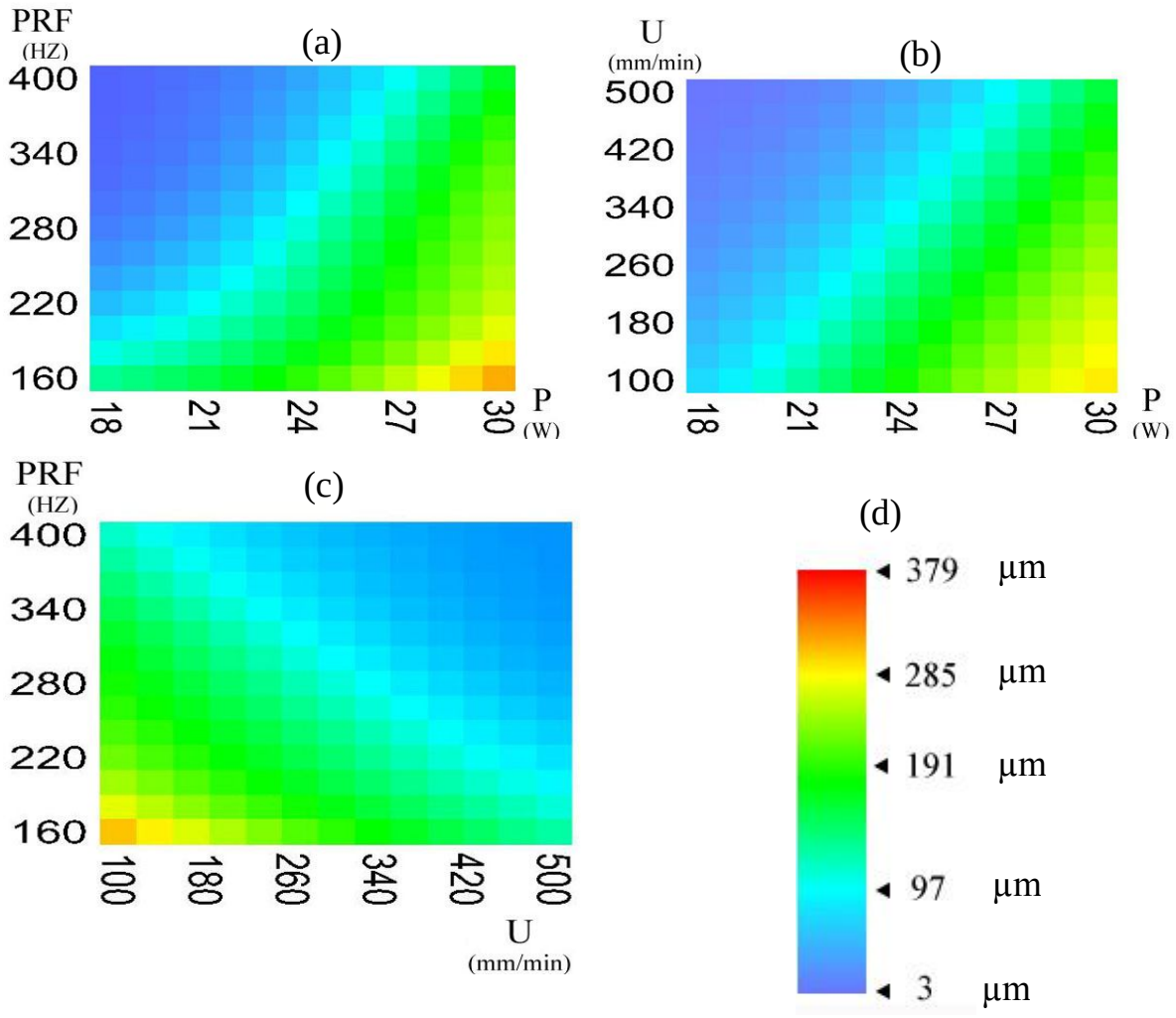

Fig. 7: Showing interactive effect on depth level for (a) PRF and P with U=300 mm/min; (b) U and P with PRF=280 Hz; (c) PRF and U with P=24W; and (d) scale bar for dimensions.

4. Discussion

Tests were performed using multilayered feed-forward, back-propagation ANNs to construct predictive models in order to predict the laser machined micro-channel geometrical parameters. Experiments designed by factorial DoE were used to develop three sets of training data and test data for three ANNs predictive models. The ANN architecture that achieved the lowest average percentage error for the test data set was chosen for each ANN predictive model, see Table 3. The predicted dimensions from the three ANN models and the DoE model were compared with the actual experimental data in terms of the average percentage error and the absolute maximum percentage error.

ANN models over time may not work as well as when they were first implemented due to deterioration of the equipment. Experimental data points can be re-captured for the chosen model in this case and used to re-train this ANN model structure with the same number of nodes and layers. In considering the range of capability and limitations, ANN predictive models are effective in predicting the process outputs for the specific materials and other input parameters used to generate the model. Furthermore, the model can be used to selected inputs for required process outputs that are within the range of the original input data used during the training phase [41]. It was found that ANNs have the inherent ability to model a nonlinear, dynamic and complicated system, such as a laser micro-machining system. In the work presented in this paper factorial DoE was an aid to the selection of training data sets for the ANN models. This was found in the works of other workers [34, 35].

Ranking the models (A, B, C and DoE) according to their average percentage error, model B produced the lowest average percentage error. The DoE model was next best in terms of having lowest average percentage error. Model B was better than model A, even though a larger number of training data was used for model A (24 for model A compared to 15 for model B). This may be due to the fact that one of the corner points from the experimental data space was missing from the training data for model A whereas model B had all the corner data points in its training data set. This indicates that the training data for model B

was the most useful training data to include and highlights the importance of including the corner points in the model. On the other hand, from Table 4, model A can be seen to have produced the lowest maximum percentage error which can be explained by the fact that this ANN model had the highest number of training data (24 from the 27 available data). This was a larger amount of training data compared to the other models and enabled this model to predict the test data set values with a smaller margin of error. The DoE model ranked second with respect to the width prediction, while model B was second regarding depth prediction. The worse prediction from model C can be understood when it is considered that four of the eight corner points from the experimental data space were excluded from training, so the prediction within the data space will not be sufficiently precise from this model.

Investigation of the combined effects of the laser control parameters is shown in the intensity plots of Fig. 6 and Fig. 7 for width and depth respectively. From these it can be seen that within the range investigated, the power has a large positive effect on the channel widths and depths. On the other hand, the PRF has a negative effect on the channel widths and depths. Traverse speed however has little effect for channel widths but some negative relation on channel depths.

Modelling all the important factors that affect the resulting dimensions of laser micro-machined components by conventional analytical or numerical methods is not currently possible. In practice when starting a new machining operation with requirement for specific part dimensions and new materials, the operator performs a set of experiments to set the process control parameters related to the laser power, PRF, motion control and work piece material. This trial-and-error approach can be costly and time consuming especially for small batch production or prototyping, and does not ensure optimal process conditions for given manufacturing objectives [26]. The results presented here allow the processing parameters to be directly selected for future work. When a particular dimension is required within the range of dimensions that have been investigated, the input parameters to achieve these can be directly selected by using model B where the minimum average error is required and model A where the minimum absolute error is required.

There are many other modelling and optimisation techniques such as genetic algorithms, ant colony optimisation, grammatical evolution, simulated annealing, tabu search, stochastic tunnelling, differential evolution, particle swarm optimization and fuzzy logic which could also be applied to such a problem. Many of these techniques are more recently developed than the ANN or DoE modelling methods. This gives some confidence in the use of ANN and DoE for problem solving as presented in this paper. However, it also opens the possibility for further research to investigate if any of these other techniques can be more easily or more successfully applied to solve such problems. ANN models can be used to predict results that were not found from experimental work. By utilisation of any of the aforementioned optimisation techniques in conjunction with the ANN models, optimised process control parameter could be found for achieving target responses, boost the process performance and improve the final product quality.

5. Conclusion

Micro-channel formation using laser micro-machining was characterised using factorial DoE. This process was modelled using feed-forward, back-propagation ANNs. The effect of different sets of training data and test data were examined. The ANN models, DoE model and experimental results were compared in terms of the average percentage error and absolute maximum percentage error. The results from this comparison showed that the ANN modelling technique can be readily applied to predict the laser machined micro-channel dimensions accurately.

Control of automated systems may require lower part absolute error or reduced overall average error. ANN models for achieving each of these requirements were established in this work. Where a small amount of scarp is acceptable or where the absolute maximum error does not stop a micro-machined part from operating in an acceptable manner, a model that produces a lower overall average error would generally be preferred. It was found that the developed ANN models are efficient predictive tool for selection of laser micro-grooving parameters.

References

[1] J. Hecht, The Laser Guidebook, first ed., McGraw-Hill, New York, 1986.

[2] N.B. Dahotre, S. Harimkar, Laser Fabrication and Machining of Materials, Springer, 2008, pp. 247-288.

[3] A. Issa, Computational control of laser systems for micro-machining, PhD Thesis, Dublin City University, Ireland, 2007.

[4] S. Juodkazis, K. Yamasaki, A. Marcinkevicius, V. Mizeikis, S. Matsuo, H. Misawa, T. Lippert, Micro-structuring of silica and polymethylmethacrylate glasses by femtosecond irradiation for Materials Science of MEMS applications, Mat. Res. Soc. Symp. Proc., 687 (2002) B5.25.1 - B5.25.6.

[5] S.C. Wang, C.Y. Lee, H.P. Chen, Thermoplastic microchannel fabrication using carbon dioxide laser ablation, Journal of Chromatography A, 1111 (2006) 252 – 257.

[6] F.G. Bachmann, Industrial laser applications, Applied Surface Science, 46 (1990) 254 – 263.

[7] M.C. Gower, Industrial applications of laser micro-machining, Optics Express, 7 (2000) 56-67.

[8] M. Goretty A.-Amigo, Polymer Micro-fabrication for Microarrays, Micro-reactors and Micro-fluidics, Journal of the Association for Laboratory Automation, 5 (2000) 96-101.

[9] M. Kamata, M. Obara, R. Gattass, L. Cerami, E. Mazur, Optical vibration sensor fabricated by femtosecond laser micro-machining, Applied Physics Letters, 87 (2005) 1-3.

[10] J.H. Strickler, W.W. Webb, Three-dimensional optical data storage in refractive media by two-photon point excitation, Optical Letters, 16 (1991) 1780 – 1782.

[11] M.H. Hong, B. Luk'yanchuk, S.M. Huang, T.S. Ong, L.H. Van, T.C. Chong, Femtosecond laser application for high capacity optical data storage. Applied Physics A: Materials Science & Processing, Springer, 79 (2004) 791–794.

[12] E.N. Glezer, M. Milosavljevic, L. Huang, R.J. Finlay, T.H. Her, J.P. Callan, E. Mazur, Three-dimensional optical storage inside transparent materials, Opt. Lett., 21 (1996) 2023-2025.

[13] www.eksma.com, EKSMA Co., Laser, optics, electronics, Glass Master Series Catalogue, accessed date: June 2008.

[14] S.H. Lee, W.S. Park, H.S. Cho, W. Zhang, M.C. Leu, A neural network approach to the modelling and analysis of stereolithography processes, Proceedings of the Institution of Mechanical Engineers, Journal of Engineering Manufacture, 215 (2001) 1719-1733.

[15] J. Ye, X.-C. Yuan, G. Zhou, Genetic algorithm for optimization design of diffractive optical elements in laser beam shaping, Proceedings of SPIE, 4594 (2003) 118-127.

[16] A.M. de Deus, J. Mazumder, Two-Dimensional Thermo-Mechanical Finite Element Model for Laser Cladding, Laser Materials Processing; Detroit, Michigan; USA, (1996) B174-B183.

[17] G.G. Wang, S.Q. Xie, Optimal process planning for a combined punch-and-laser cutting machine using ant colony, International Journal of Production Research, 43 (2005) 2195 – 2216.

[18] H. Shen, YJ. Shi, ZQ Yao, J. Hu, Fuzzy logic model for bending angle in laser forming, Materials Science and Technology, 22 (2006) 981-986.

[19] K.Y. Benyounis, A.G. Olabi, optimization of different welding processes using statistical and numerical approaches–A reference guide, Advances in Engineering Software, Elsevier, (2008) 483–496.

[20] E.M. Anawa, A.G. Olabi, Using Taguchi method to optimize welding pool of dissimilar laser-welded components, Optics and Laser Technology, Elsevier, 40 (2008) 379–388.

[21] A.G. Olabi, G. Casalino, K.Y. Benyounis, M.S.J. Hashmi. An ANN and Taguchi algorithms integrated approach to the optimization of CO2 laser welding, Advances in Engineering Software, Elsevier, 37 (2006) 643–648.

[22] www.academic.marist.edu/~jzbv/architecture/Projects/S2002/NeuralNet2/COA.PPT, accessed date: May 2008.

[23] http://www.cormactech.com/neunet/whatis.html, What is a Neural Net? - A Brief Introduction, accessed date: May 2008.

[24] V. Dragos, V. Dan, R. Kovacevic, Prediction of the laser sheet bending using neural network, Proceedings of Circuits and Systems, ISCAS, Geneva, (2000) III686-III689.

[25] D. Dhupal, B. Doloi, B. Bhattacharyya, Optimization of process parameters of Nd-YAG laser micro-grooving of Al_2TiO_5 ceramic material by response surface methodology

and artificial neural network algorithm, Proc. IMechE, Part B: J. Engineering Manufacture 221 (2007) 1341 – 1351.

[26] B.F. Yousef, G.K. Knopf, E.V. Bordatchev, S.K. Nikumb, Neural network modelling and analysis of the material removal process during laser machining, Int J Adv Manuf Techno, 22 (2002) 41 -53.

[27] R. Setia, G.S. May, Modeling and optimization of via formation in dielectrics by laser ablation using neural networks and genetic algorithms, IEEE transactions on electronics packaging manufacturing, 27:22 (2004) 133-144,.

[28] S. Zurek, P. Marketos, A.J. Moses, LabVIEW as a tool for measurements, batch data manipulations and artificial neural network predictions, Przeglad Elektrotechniczny, 83 (4/2007) 114-119.

[29] S. Zurek, A.J. Moses, M. Packianather, P. Anderson, F. Anayi, Prediction of power loss and permeability with the use of an artificial neural network in wound toroidal cores Journal of Magnetism and Magnetic Materials, 320 (2008) 1001-1005.

[30] S. Haykin, Neural Networks : A comprehensive foundation, MacMillan College Publishing, New York, 1994.

[31] A. Vaidyanathan, T. W. Walker, A. H. Guenther, The relative roles of avalanche multiplication and multiphoton absorption in laser-induced damage of dielectrics, IEEE Journal of Quantum Electronics, QE-16 (1980) 89-93.

[32] Y.-I. Lee, K. Song, J. Sneddon, Laser-induced breakdown spectrometry, Nova Science publishers, Inc., New York, 2000.

[33] A. Issa, D. Brabazon, S. Hashmi, 3D transient thermal modelling of laser microchannel fabrication in lime-soda, Journal of Materials Processing Technology, 207 (2008) 307-314.

[34] P.P. Balestrassi, E. Popova, A.P. Paiva, J.W. Lima, Design of experiments on neural network's training for nonlinear time series forecasting, Neurocomputing, Elsevier, 72 (2009) 1160-1178.

[35] K. Omata, Y. Watanabe, M. Hashimoto, T. Umegaki, M. Yamada, Optimization of Cu-based Oxide Catalyst for Methanol Synthesis Using a Neural Network Trained by Design of Experiment, Journal of the Japan Petroleum Institute, 46 (2003) 387－391.